

# Do Leonardo Da Vinci's Drawings, Room Acoustics And Radio Astronomy Have Anything In Common?

Andrzej Kulowski (✉ [kulowski@pg.edu.pl](mailto:kulowski@pg.edu.pl))

Gdańsk University of Technology <https://orcid.org/0000-0001-7003-9515>

---

## Research Article

**Keywords:** Leonardo da Vinci, caustic, spherical reflector, room acoustics, Arecibo, FAST

**Posted Date:** January 3rd, 2022

**DOI:** <https://doi.org/10.21203/rs.3.rs-1206026/v1>

**License:**  This work is licensed under a Creative Commons Attribution 4.0 International License.

[Read Full License](#)

---

1 Do Leonardo da Vinci's drawings, room acoustics and radio astronomy

2 have anything in common?

3

4 Andrzej Kulowski, Gdańsk University of Technology, Faculty of Architecture,

5 ul. Gabriela Narutowicza 11/12, 80-233 Gdańsk, Poland, e-mail: kulowski@pg.edu.pl

6 ORCID: 0000-0001-7003-9515

7

### Abstract

8

9 After introducing Leonardo da Vinci's (LdV) predecessors in the field of light propagation

10 research, his drawings on the topic of focussing light through a spherical mirror are analysed.

11 The discovery of LdV is presented, according to which, at an infinitely distant source of rays,

12 a small fragment of the canopy is enough to generate a focus, while the rest of the mirror

13 forms caustics for which LdV did not indicate an application. An analytical description of the

14 energy concentration in the focus and on the caustics is given, together with its reference to

15 the geometric representation of the acoustic field in rooms. Using symmetry in the description

16 of energy relations in acoustics and electromagnetism, the interference that occurs on the

17 caustics produced by the acoustic and electromagnetic wave is discussed. It is explained why

18 in the sound field in existing halls, instead of a whole caustic only its cusp is observed, which

19 is perceived as a point-like sound focus. The size of the mirror aperture, shown graphically by

20 LdV, is determined. How the development of receiving techniques increased the mirror aper-

21 ture compared to the LdV estimate is also shown. The implementation of these improvements

22 is presented via the example of the Arecibo and FAST radio telescopes.

23 Key words:

24 Leonardo da Vinci, caustic; spherical reflector; room acoustics; Arecibo; FAST

25

26

27

## 28 **1.Introduction**

29           Early considerations about the propagation of light lie at the beginning of the research  
30 discipline that has developed into today's physics. One of the earliest accounts on optics, i.e.  
31 the use of instruments interfering with the course of light, is the story from ancient times  
32 about Archimedes setting fire to Roman ships besieging Carthage with the use of mirrors re-  
33 flecting sunlight [1]. A later treatise by Ptolemy from the 2nd century AD is another signifi-  
34 cant work of the antiquity period concerning the study of optics [2]. The scientific considera-  
35 tions he initiated were continued in the Middle Ages in the Islamic world. Leonardo da Vinci  
36 (LdV) carried out his works in reference to this tradition [3]. He paid particular attention to  
37 the application of the rules of geometric optics in architecture, painting and graphics, includ-  
38 ing studies in the field of perspective and chiaroscuro.

39           Leonardo's sketches on optics include studies of a particular form of focussing rays of  
40 light, nowadays known as caustics. In the convention of geometric optics, caustics is a surface  
41 formed by rays tangent to it after reflection from a concave surface or as a result of propaga-  
42 tion in an inhomogeneous medium. Under certain circumstances, a cusp may form on the  
43 caustics. In the mathematical description of caustics, it corresponds to a singularity, i.e. the  
44 parameters of the field of rays at this point tend to infinity. The physical counterpart of the  
45 caustic cusp is the focus of the mirror. The focus can also form without a caustic accompany-  
46 ing it, but it only applies to a few specific cases, among them a source in the centre of a spher-

47 ical reflector, a parabolic reflector with an infinitely distant source on its geometric axis, or an  
48 ellipsoidal reflector with a source in one of its foci.

49 Leonardo showed that with an infinitely distant light source, only a small part of the  
50 spherical mirror is involved in creating the focus. The remainder of the mirror only forms  
51 caustics and is useless for focal formation, leading to important practical conclusions. The  
52 idea of focussing light in this way is attributed to Archimedes, who lived many centuries ear-  
53 lier, but the quantitative analysis shown graphically in Fig. 2 is Leonardo's personal contribu-  
54 tion to the study of the principle of the operation of a concave mirror.

55 Against this historical background, the article discusses the formation of foci and caus-  
56 tics in the acoustic field and in the electromagnetic field. Observations of room acoustics indi-  
57 cate that in the audible frequency range, caustics are so blurred by diffuse sound, wave reflec-  
58 tions and interference that it is reduced to its singularity. The observed form of caustics is then  
59 a point-like focus of sound. This occurs when the wavelength is of the same order or slightly  
60 shorter than that of the objects in the acoustic field, which is typical for rooms.

61 When the wavelength is much shorter than the objects in the wave field, the blur effect  
62 is much smaller and the caustics act as a clearly identified energy focus area. Caustics formed  
63 in this way are present in many fields of technology and science concerning the propagation  
64 of light, ultrasounds and electromagnetic waves, e.g. hydroacoustics, aeroacoustics, laser  
65 technology, and even radio astronomy [4], [5], [6].

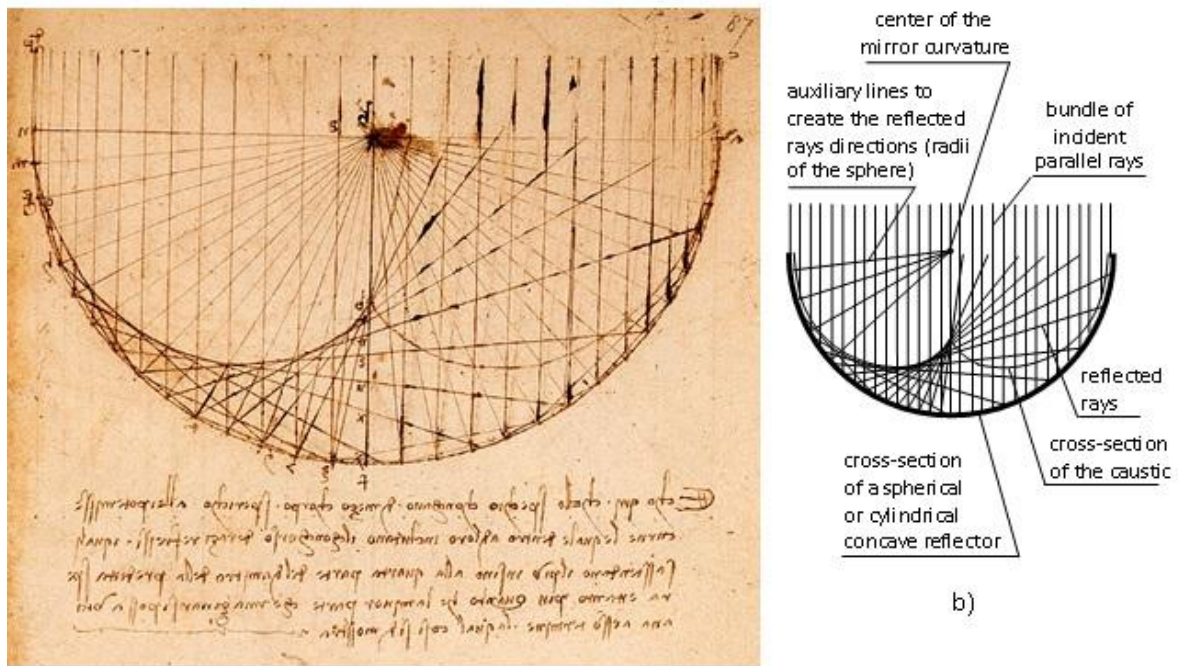
66           Based on the inspiration of caustic drawings in LdV's works and his considerations on  
67 focussing light by a concave mirror, the article presents a mathematical description of the ef-  
68 fect of focussing rays. Against this background, the phenomena occurring on caustics in  
69 acoustic and electromagnetic fields are presented, taking into account their wave nature.

70           The main goal of this paper is to investigate the extent to which LdV observations of  
71 the formation of caustics and foci are present in modern technology. The article shows how  
72 LdV's estimate of a mirror aperture has expanded as radio waves receiving techniques have  
73 developed. The presence of Leonard's thoughts in these activities is demonstrated through the  
74 example of the large radio telescopes in Arecibo (Puerto Rico) and Dawodang (China).

75

## 76 **2. Caustics in the legacy of Leonardo da Vinci**

77           The drawings of caustics in Leonardo da Vinci's notes refer to his research in the field  
78 of optics in the years 1510–1515 [7], [8]. You can find in them many sketches of caustics at  
79 different stages of their formation, the most complete drawing of caustics is shown in Fig. 1.  
80 Leonardo made his drawing 500 years ago with such competence that in the article it is quot-  
81 ed as a perfectly valid example of applying the principles of geometric optics in the formation  
82 of caustics.



a)

b)

c)

d)

83

84 Fig. 1. a) Drawing of caustic from Leonardo da Vinci's sketchbook. The note below the picture in Fig.

85 1a, made in Leonardo's famous reverse script, says that in concave mirrors of equal diameter, the one

86 that has the shallower curve will concentrate the largest number of reflected rays onto a focal point,

87 and "as a consequence, it will kindle a fire with greater rapidity and force" [9]. b) Details of Leonar-

88 do's drawing, c), d) 3D views of the caustics created by spherical and cylindrical concave mirrors [10].

89

90

91

92 Leonardo was interested in the potential utility of concave mirrors as sources of heat,  
 93 and the purpose of his research was to assess the focussing properties of a spherical mirror.  
 94 Fig. 2 shows the two mirrors differing in the depth of the canopy referred to in his reverse  
 95 script in Fig. 1a. In his later works, Leonardo also planned to use the effect of focussing sun-  
 96 light to heat or even boil water [11].

97 In light of today's level of knowledge, Leonardo's concept is obvious. However, he  
 98 lived 500 years ago and the accuracy of his explanations must be considered admirable. The  
 99 further part of the article shows that even in areas as distant from optics as room acoustics and  
 100 radio astronomy, Leonardo da Vinci's concept can be found.

101 According to modern technical terminology, the fraction of the total energy incident  
 102 on the mirror that is available at the receiver is called the mirror aperture. For the purposes of  
 103 this article, the ratio of this area to the area of a full hemispherical mirror was adopted as the  
 104 relative measure of aperture. Assuming the propagation and reflection of the rays are lossless,  
 105 the relative aperture of the lower mirror shown in Fig. 2 is approximately 0.4% (Eqs. (1), (2)).

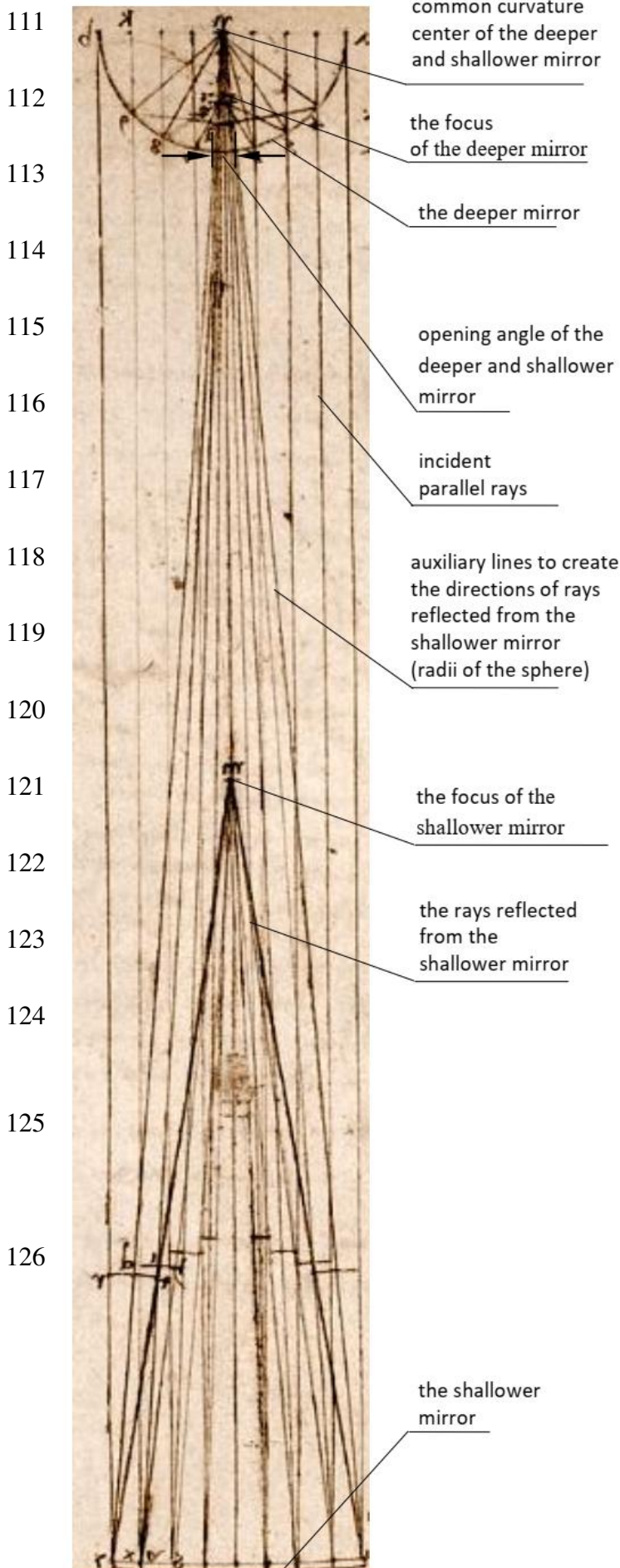
106 For the opening angle  $\varphi = 10^\circ$  (Fig. 3), the arc length  $r$  is

$$107 \quad r = \frac{\varphi/2}{180} \Pi R = \frac{\Pi R}{36} \quad (1)$$

108 and the aperture in relation to the surface of the full hemispherical mirror is

$$109 \quad \frac{S_a}{S_m} = \frac{\Pi r^2}{2\Pi R^2} = \frac{1}{2} \left( \frac{\Pi}{36} \right)^2 = 0.0038 \cong 0.4\% \quad (2)$$

110



### 3. Analytic description of energy

#### concentration on the caustic

The LdV sketches present the effect of the energy concentration on a caustic in a graphical form. This section gives a quantitative assessment of this effect in an analytical form, using the original LdV drawing.

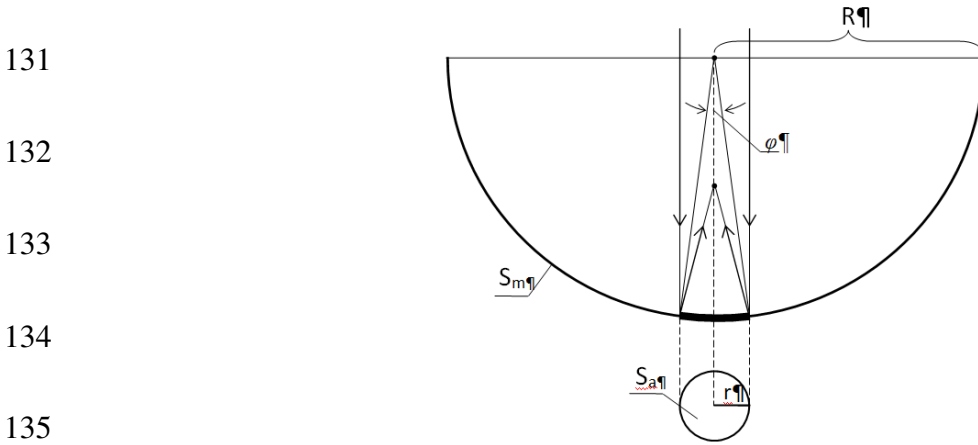
Consider the rays coming from an infinitely distant source and falling on a hemispherical mirror as a collimated beam (Fig. 1a). After the reflection, the rays form the caustic described by Eq. (3) [12].

$$\begin{cases} x(\theta) = R \cos^3(\theta) \\ y(\theta) = \frac{R}{2} (2 \sin^3(\theta) - 3 \sin(\theta)) \end{cases} \quad 0 \leq \theta \leq \Pi \quad (3)$$

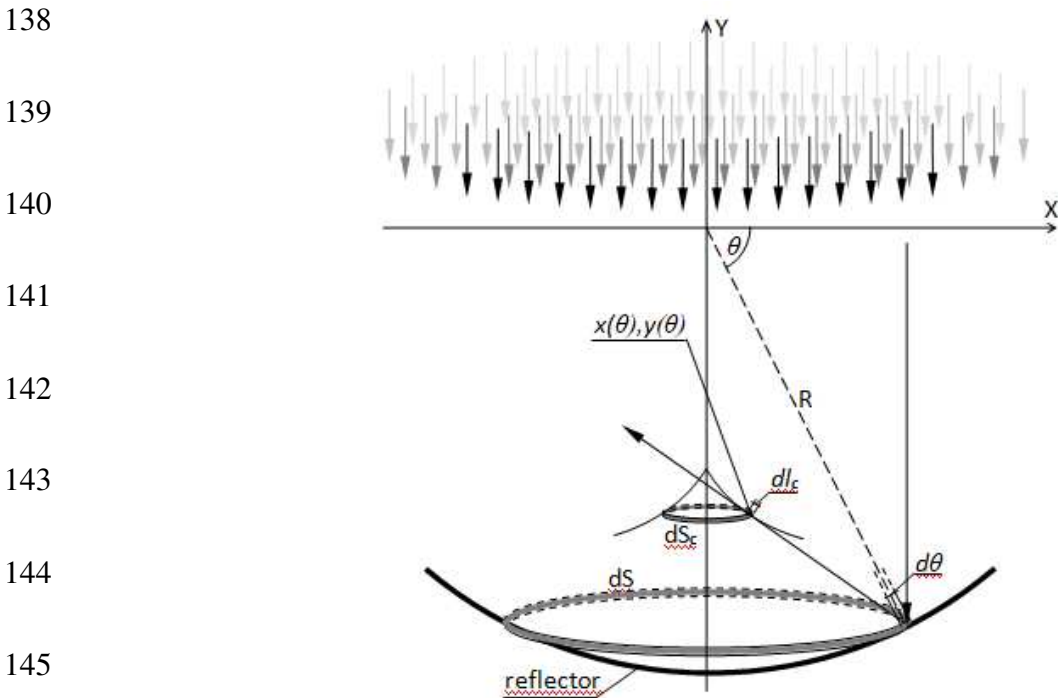
Fig. 2. Illustration of Leonardo's concept, in which a shallower mirror (bottom) concentrates a larger number of rays than the mirror with a deeper bowl of the same diameter (top) [9].



127 To calculate the density of rays on a caustic, consider two rings inside the reflector's  
 128 bowl:  $dS$  on its surface and  $dS_c$  on a caustic (Fig. 4) [12], [13]. Since all rays reflected from  $dS$   
 129 are tangent to  $dS_c$ , the density of rays on  $dS_c$  is  $dS/dS_c$ , where  $dS$  and  $dS_c$  are the surfaces of the  
 130 rings.



136 Fig. 3. Aperture of the shallower mirror from Fig. 2.  $S_m$ ,  $R$ : area and radius of the full hemispherical mir-  
 137 ror,  $S_a$ ,  $r$ : area and radius of the aperture,  $\varphi$ : opening angle read from Fig. 2,  $\varphi = 10^\circ$ .



146 Fig. 4. Caustic formed by rays incident on a hemispherical reflector.  $R$ : radius of the reflector,  
 147  $dS$ ,  $dS_c$ : ring on the reflector and on the caustic,  $x(\theta), y(\theta)$ : Cartesian coordinates of the caustic

(Eq. (3)),  $dl_c$ : the element of the section of the caustic [13]

148 The circumference and the width of the ring  $dS$  are  $2\Pi R \cos(\theta)$  and  $R \sin(\theta) d\theta$ , so

$$149 \quad dS = 2\Pi R^2 \cos(\theta) \sin(\theta) d\theta \quad (4)$$

150 Likewise, the circumference and the width of the ring  $dS_c$  are  $2\Pi x(\theta)$  and  $dl_c$ , so

$$151 \quad dS_c = 2\Pi x(\theta) dl_c \quad (5)$$

152 where  $dl_c$  is the element of a section of a caustic

$$153 \quad dl_c = \sqrt{\left(\frac{dx(\theta)}{d(\theta)}\right)^2 + \left(\frac{dy(\theta)}{d(\theta)}\right)^2} d\theta \quad (6)$$

154 and the derivatives over  $\theta$  of  $x(\theta)$ ,  $y(\theta)$  are

$$155 \quad \begin{cases} \frac{dx}{d\theta} = -3R \cos^2(\theta) \sin(\theta) \\ \frac{dy}{d\theta} = 3R \sin^2(\theta) \cos(\theta) - \frac{3}{2} R \cos(\theta) \end{cases} \quad (7)$$

156 An elementary transformation gives

$$157 \quad \sqrt{\left(\frac{dx(\theta)}{d(\theta)}\right)^2 + \left(\frac{dy(\theta)}{d(\theta)}\right)^2} = \frac{3}{2} R \cos(\theta) \quad (8)$$

158 Substitution of Eq. (7) to Eq. (6) yields

$$159 \quad dl_c = \frac{3}{2} R \cos(\theta) d\theta \quad (9)$$

160 so

$$dS_c = 3\Pi R^2 \cos^4(\theta) d\theta \quad (10)$$

161 Finally, if the rays incident on the mirror are distributed evenly on the  $y = 0$  plane (Fig. 4), the

162 density of rays  $C(\theta)$  over the caustic is

$$163 \quad C(\theta) = \frac{dS}{dS_c} = \frac{2 \sin(\theta)}{3 |\cos^3(\theta)|} \quad (11)$$

164 As  $\theta$  tends to  $0.5\Pi$ ,  $C(\theta)$  tends to infinity, which corresponds to the cusp formation on the  
 165 caustic (Fig. 4). This singularity results from the caustic cross-sectional area  $dS_c$  tending to  
 166 zero.

167 Let us denote the surface density of rays incident on the reflector as  $I_0$  [ $\text{W}/\text{m}^2$ ]. The  
 168 density of rays  $C(\theta)$  in Eq. (11) multiplied by  $I_0$  can be interpreted as the surface density of  
 169 energy over the caustic per unit of time, i.e. the intensity of the rays [ $\text{W}/\text{m}^2$ ]. When the ab-  
 170 sorption coefficient  $\alpha$  of the reflector is taken into account, where  $\alpha = 0$  and  $\alpha = 1$  relate to a  
 171 total reflection and total absorption, respectively, the rays intensity is

$$172 \quad I_c(\theta) = I_0(1-\alpha) C(\theta) = I_0(1-\alpha) \frac{2\sin(\theta)}{3|\cos^3(\theta)|} \quad [\text{W}/\text{m}^2]. \quad (12)$$

173 The total intensity of the rays over the caustic  $I_{c,res}(\theta)$  consists of the energy of incident rays  $I_0$   
 174 and the energy of the reflected rays condensed on the caustic.

$$175 \quad I_{c,res}(\theta) = I_0 + I_0(1-\alpha) \frac{2\sin(\theta)}{3|\cos^3(\theta)|} = I_0 \left( 1 + (1-\alpha) \frac{2\sin(\theta)}{3|\cos^3(\theta)|} \right) \quad (13)$$

176 The intensity level of the rays on the caustic, with  $I_0$  as the reference intensity, is then  $L_{c,res}(\theta)$   
 177 (Fig. 5).

$$178 \quad L_{c,res}(\theta) = 10 \log \frac{I_{c,res}(\theta)}{I_0} = 10 \log \left( 1 + (1-\alpha) \frac{2\sin(\theta)}{3|\cos^3(\theta)|} \right) \quad [\text{dB}] \quad (14)$$

179

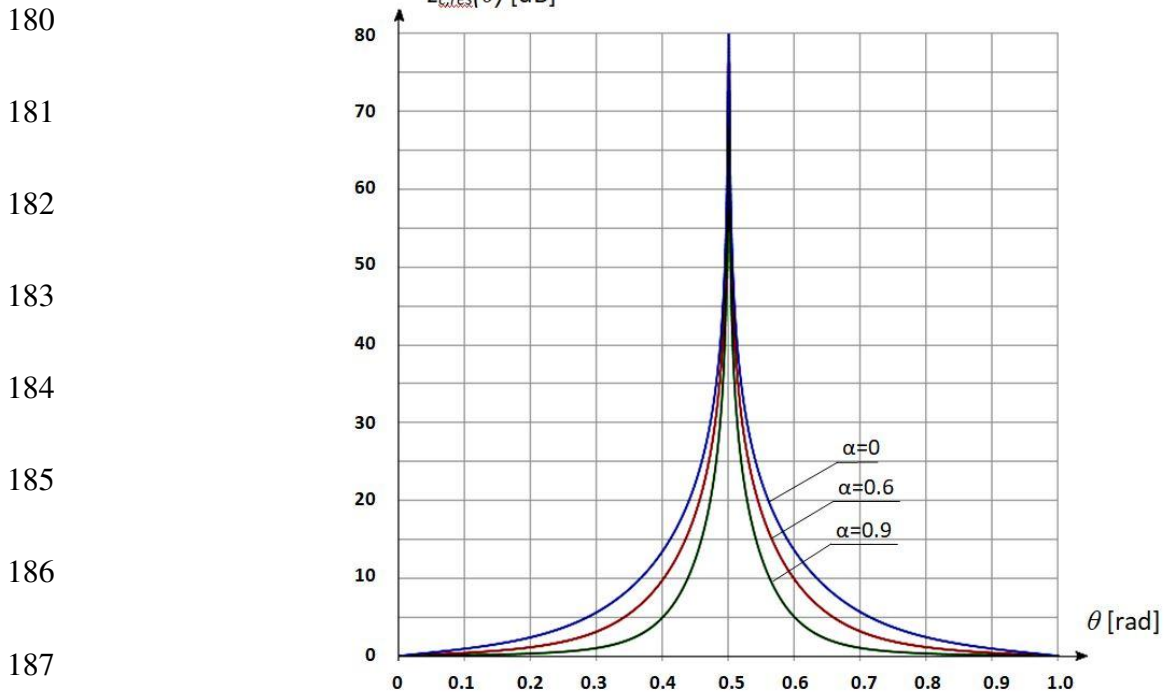


Fig. 5. Rays' intensity level  $L_{c,res}(\theta)$  [dB] on the caustic.

$\alpha$ : absorption coefficient of the reflector [12].

190

#### 191 4. Caustics in the wave field

192

LdV's concept of caustics and its development, as shown in Fig. 2 and section 3, are

193

based on the geometrical approach. Despite the roots that are distant in time, this approach is

194

a fully functional model of energy propagation, currently used, for example, in room acous-

195

tics, optics and radio communication. This section describes the formation of caustics in a

196

wave field, the manifestation of which is the interference of the incident wave with the wave

197

reflected from the mirror.

198

Let us consider a plane wave of the wavelength  $\lambda$  much smaller than the diameter of

199

the reflector  $D$ , incident on the reflector [12]. At the point in time  $t = 0$ , the wave front lies in

200 the plane  $y = 0$  (Fig. 6). Propagating deep into the reflector, the wave interferes with the re-  
 201 flected wave. According to the law of reflection, the reflected wave is tangent to the caustic.

202 The distances SKN and SLMN travelled by the incident and reflected waves are

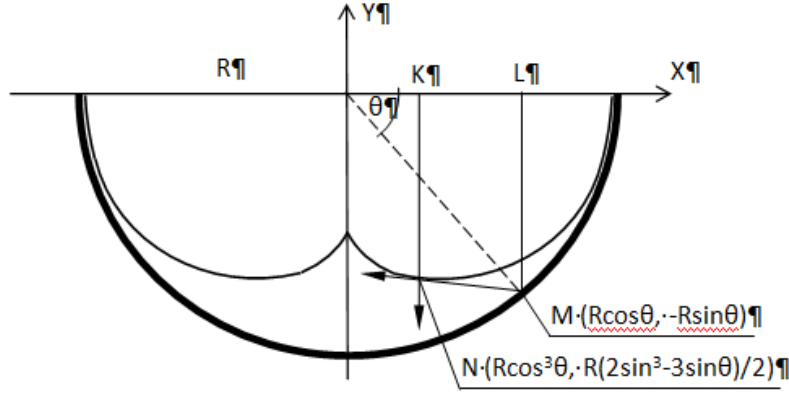
$$203 \quad S_{KN} = \frac{R}{2} |2\sin^3 \theta - 3\sin \theta| = \frac{R}{2} (3\sin \theta - 2\sin^3 \theta), \quad 0 \leq \theta \leq \pi \quad (15)$$

$$S_{LMN} = R\sin \theta + \sqrt{(R\cos \theta - R\cos^3 \theta)^2 + \left(-R\sin \theta - \left(\frac{R}{2}(2\sin^3 \theta - 3\sin \theta)\right)\right)^2} = R\sin \theta + \sqrt{\left(\frac{R}{2}\sin \theta \sin 2\theta\right)^2 + \left(\frac{R}{2}\sin \theta \cos 2\theta\right)^2} =$$

$$204 \quad R\sin \theta + \frac{R}{2}\sin \theta \sqrt{(\sin 2\theta)^2 + (\cos 2\theta)^2} = \frac{3}{2}R\sin \theta, \quad 0 \leq \theta \leq \pi \quad (16)$$

206

207



208

209

210

211 Fig. 6. Directions of the incident and reflected waves KN and LMN overlapping

212

each other on the caustics. R: radius of the reflector [12]

213

214

In spite of the essentially different nature of acoustic and electromagnetic waves, the

215

general principles of wave motion describe the energetic relationships of acoustic and elec-

216

tromagnetic waves using the same equations, differing only in the physical interpretation of

217

the individual components. To highlight this similarity, successive equations relating to

218

acoustic and electromagnetic fields are presented side-by-side.

219 The sound intensity  $I_s$  and surface power density of the electromagnetic field  $I_e$ , both  
 220 in  $[\text{W}/\text{m}^2]$ , are proportional to the squared sound pressure  $p^2$  [Pascal] and squared intensity of  
 221 the electric field  $E$  [V/m], respectively

$$222 \quad I_s = p^2/(\rho c_s) \quad I_e = E^2/(\mu_0 c_l) \quad (17), (18)$$

223 where:

224  $\rho$ : density of the medium,  $[\text{kg}/\text{m}^3]$ ,

225  $c_s$ : speed of sound (in the air at atmospheric pressure and a temperature of  $15^\circ\text{C}$ ,  $c_s = 331$  m/s,

226  $\rho c_s = 415[\text{kg}/(\text{m}^2\text{s})]$ ).

227  $\mu_0$ : vacuum permeability ( $\mu_0 = 4\pi 10^{-7}$ , [H/m]),

228  $c_l$ : speed of light ( $c_l = 3 \cdot 10^8$  [m/s]).

229

230 So the amplitude of the sound pressure  $\overline{p_c(\theta)}$  and the amplitude  $\overline{E_c(\theta)}$  of the electric field's in-

231 tensity condensed on the caustic are

$$232 \quad \overline{p_c(\theta)} = \sqrt{I_{c,s}(\theta)\rho c_s} = \sqrt{I_o\rho c_s} \sqrt{\frac{2(1-\alpha)\sin(\theta)}{3|\cos^3(\theta)|}} \quad \overline{E_c(\theta)} = \sqrt{I_{c,em}(\theta)\mu_0 c_l} = \sqrt{I_{em}\mu_0 c_l} \sqrt{\frac{2\mathcal{R}\sin(\theta)}{3|\cos^3(\theta)|}} \quad (19), (20)$$

233 where:

234  $I_{c,s}(\theta)$ : sound intensity on the caustic,  $[\text{W}/\text{m}^2]$ ,

235  $I_{c,em}(\theta)$ : surface power density of the electromagnetic field on the caustic,  $[\text{W}/\text{m}^2]$ ,

236  $I_o$ : intensity of the incident sound,  $[\text{W}/\text{m}^2]$ ,

237  $I_{em}$ : surface power density of the electromagnetic field, of the incident wave,  $[\text{W}/\text{m}^2]$ .

238  $\alpha$ : sound absorption coefficient,

239  $\mathcal{R}$ : reflection coefficient of the electric component of the electromagnetic wave.

$$240 \quad \alpha = \frac{I_{\text{abs}}}{I_i} = \left( \frac{\overline{P_{\text{abs}}}}{\overline{P_i}} \right)^2 \quad \mathcal{R} = \left( \frac{\overline{E_{\text{refl}}}}{\overline{E_i}} \right)^2 \quad (21), (22)$$

241  $I_{\text{abs}}, I_i$ : intensity of the absorbed and incident acoustic wave,

242  $\overline{p_i}, \overline{P_{\text{abs}}}$ : sound pressure amplitude of the incident and absorbed acoustic wave,

243  $\overline{E_i}, \overline{E_{\text{refl}}}$ : amplitude of the incident and reflected intensity of the electric field. For the sake of

244 brevity, the total reflection of the electromagnetic wave, i.e.  $\mathcal{R} = 1$ , was adopted in

245 the article.

246

247 Attention is drawn to the different meanings of the word “intensity” in acoustics and electro-

248 magnetism. “Intensity of the acoustic field” is proportional to  $p^2$  (Eq.17)), while “intensity of

249 electric field” refers to  $E$  in the first power (Eq.(20). The quantity proportional to  $E^2$  is called

250 the “surface power density of the electromagnetic field” (Eq.18)).

251 At the point in time  $t$ , the sound pressure  $p_i(t)$  and the intensity of the electric field  $E(t)$

252 of the incident acoustics and electromagnetic wave, respectively, in the plane  $y = 0$  of the re-

253 flector are

$$254 \quad p_i(t) = \sqrt{I_0 \rho c_s} \sin \omega t \quad E(t) = \sqrt{I_{\text{em}} \mu_0 c_t} \sin \omega t \quad (23), (24)$$

255 where:

256  $\omega = 2\pi f$ ,  $f$ : frequency, [Hz].

257 Assuming lossless wave propagation, after travelling the distance  $S_{KN}$  by the acoustic  
 258 wave, the sound pressure is

$$259 \quad p_{KN}(t) = \sqrt{I_0 \rho c_s} \sin \varpi(t + \Delta t_{1,s}), \quad \Delta t_{1,s} = S_{KN}/c_s \quad (25), (26)$$

260 and after travelling the distance  $S_{LMN}$  and wave condensation on the caustic according to Eq. (19)

$$261 \quad p_{LMN}(t, \theta) = \sqrt{I_0 \rho c_s} \sqrt{\frac{2(1-\alpha)\sin(\theta)}{3|\cos^3(\theta)|}} \sin \varpi(t + \Delta t_{2,s}), \quad \Delta t_{2,s} = S_{LMN}/c_s \quad (27), (28)$$

262 Similarly, after travelling the distance  $S_{KN}$  by the electromagnetic wave the intensity of the  
 263 electric field  $E_{KN}(t)$  is

$$264 \quad E_{KN}(t) = \sqrt{I_{em} \mu_0 c_\ell} \sin \varpi(t + \Delta t_{1,\ell}), \quad \Delta t_{1,\ell} = S_{KN}/c_\ell \quad (29), (30)$$

265 and after travelling the distance  $S_{LMN}$  and wave condensation on the caustic according to Eq. (20)

$$266 \quad E_{LMN}(t, \theta) = \sqrt{I_{em} \mu_0 c_\ell} \sqrt{\frac{2\sin(\theta)}{3|\cos^3(\theta)|}} \sin \varpi(t + \Delta t_{2,\ell}), \quad \Delta t_{2,\ell} = S_{LMN}/c_\ell \quad (31), (32)$$

267 The resultant sound pressure  $p_{c,res}(t, \theta)$  [Pa] and intensity of the electric field  $E_{c,res}(t)$  [V/m] on  
 268 the caustic are then

$$269 \quad p_{c,res}(t, \theta) = \sqrt{I_0 \rho c_s} \left( \sin \varpi(t + \Delta t_{1,s}) + \sqrt{\frac{2(1-\alpha)\sin(\theta)}{3|\cos^3(\theta)|}} \sin \varpi(t + \Delta t_{2,s}) \right) \quad (33)$$

$$270 \quad E_{c,res}(t, \theta) = \sqrt{I_{em} \mu_0 c_\ell} \left( \sin \varpi(t + \Delta t_{1,\ell}) + \sqrt{\frac{2\sin(\theta)}{3|\cos^3(\theta)|}} \sin \varpi(t + \Delta t_{2,\ell}) \right) \quad (34)$$

271 The phase difference  $\Delta t_1 - \Delta t_2$  in Eqs. (33) and (34) increases with  $\theta$ , which causes  $p_{c,res}(t)$  and  
 272  $E_{c,res}(t)$  to fluctuate on the caustic over time. Fluctuations of sound pressure are described by  
 273 Eq. (35), which is obtained by substituting equations (15), (16) to (26), (28) and then to (33).



274 Fluctuations of the intensity of an electric field are described by Eq. (36) which is obtained by  
 275 substituting equations (15), (16) to (30), (32) and then to (34).

$$276 \quad p_{c,res}(t,\theta) = \sqrt{I_0 \rho c_s} \left[ \sin \varpi \left( t + \frac{R}{2c_s} (3\sin\theta - 2\sin^3\theta) \right) + \sqrt{\frac{2(1-\alpha)\sin\theta}{3|\cos^3(\theta)|}} \sin \varpi \left( t + \frac{3R}{2c_s} \sin\theta \right) \right] \quad (35)$$

$$277 \quad E_{c,res}(t,\theta) = \sqrt{I_{em} \mu_0 c_l} \left[ \sin \varpi \left( t + \frac{R}{2c_l} (3\sin\theta - 2\sin^3\theta) \right) + \sqrt{\frac{2\sin\theta}{3|\cos^3(\theta)|}} \sin \varpi \left( t + \frac{3R}{2c_l} \sin\theta \right) \right] \quad (36)$$

278 The fluctuations are in the form of amplitude modulation, the maximum range of  
 279 which results from Eqs. (37) and (38) for acoustic and electromagnetic fields, respectively.

$$280 \quad \frac{d}{dt} p_{c,res}(t,\theta) = 0 \quad \frac{d}{dt} E_{c,res}(t) = 0 \quad (37), (38)$$

281 For a given  $\theta$ , Eqs. (35) and (36) describe the fluctuations at a given point of the caustic. Solv-  
 282 ing Eqs. (37) and (38), i.e. finding the function  $t(\theta)$ , determines the amplitude of the fluctua-  
 283 tions on the entire caustics (Eqs. (39) and (40)). The solution of Eq. (37) is given in the ap-  
 284 pendix in Eq. (A9), and the solution of Eq. (38) is analogous.

$$285 \quad t_s = \frac{1}{\varpi} \arctg(q_s) - \Delta t_1 \quad t_l = \frac{1}{\varpi} \arctg(q_l) - \Delta t_1 \quad (39), (40)$$

$$286 \quad \text{where } q_s = \frac{\sqrt{\frac{3|\cos^3\theta|}{2(1-\alpha)\sin\theta} + \cos\left(\frac{R\sin^3\theta}{c_s}\right)}}{\sin\left(\frac{R\sin^3\theta}{c_s}\right)} \quad q_l = \frac{\sqrt{\frac{3|\cos^3\theta|}{2(1-\alpha)\sin\theta} + \cos\left(\frac{R\sin^3\theta}{c_l}\right)}}{\sin\left(\frac{R\sin^3\theta}{c_l}\right)} \quad (41), (42)$$

287 Substituting  $t_s$  and  $t_l$  into Eqs. (35) and (36), respectively, yields the maximum range of ampli-  
 288 tude modulation of sound pressure  $p_{c,res,Max}(\theta)$  [Pa] and intensity of electric field  $E_{c,res,Max}(\theta)$   
 289 [V/m] over the whole caustic.

$$290 \quad p_{c,res,Max}(\theta) = \sqrt{I_0 \rho c_s} \left[ \sin(\arctg(q_s)) + \sqrt{\frac{2(1-\alpha)\sin\theta}{3|\cos^3(\theta)|}} \sin\left(\arctg(q_s) + \frac{R\sin^3\theta}{c_s}\right) \right] \quad (43)$$

$$E_{c, res, Max}(\theta) = \sqrt{I_{em} \rho c_s} \left[ \sin(\arctg(q_\ell)) + \sqrt{\frac{2 \sin \theta}{3 |\cos^3(\theta)|}} \sin \left( \arctg(q_\ell) + \varpi \frac{R \sin^3 \theta}{c_\ell} \right) \right] \quad (44)$$

292

## 293 5. Case studies

294 The mechanism of caustic formation and the circumstances of the focal formation,  
 295 graphically shown by LdV in Fig. 1a, are shown in this section on real objects. The presented  
 296 examples concern the formation of caustics indoors and in outdoor acoustic installations with  
 297 a demonstration function. How the development of the receiving technique related to the de-  
 298 tection of radio waves extended the mirror aperture estimated by LdV is also shown.

299

### 300 5.1. Caustics in sound fields

301 Fig. 7 a, b presents the graph of Eq. (43) for sound waves with a frequency of  $f = 1000$   
 302 Hz and  $f = 2000$  Hz, reflected by a hemispherical reflector with the diameter of  $D = 2$  m. In  
 303 both cases, the wavelength  $\lambda$  is much smaller than the diameter of the reflector  $D$  ( $\lambda/D = 0.17$   
 304 and  $\lambda/D = 0.085$ , respectively). The directions of these waves shown in Fig. 6 therefore meet  
 305 the principles of geometric optics, and the diffraction of the wave at the reflector's edge can  
 306 be neglected.

307 Let us assume that the intensity of the incident wave  $I_0$  is  $10^{-8}$  [W/m<sup>2</sup>], which corre-  
 308 sponds to sound pressure with an amplitude of 0.002 [Pa] and sound pressure level  $SPL_i = 40$   
 309 dB re.  $2 \times 10^{-5}$  [Pa] (Eq.(45), (46)).

$$\bar{p}_i = \sqrt{I_0 \rho c_s} = \sqrt{10^{-8} * 415} \cong 0.002 \text{ [Pa]} \quad (45)$$

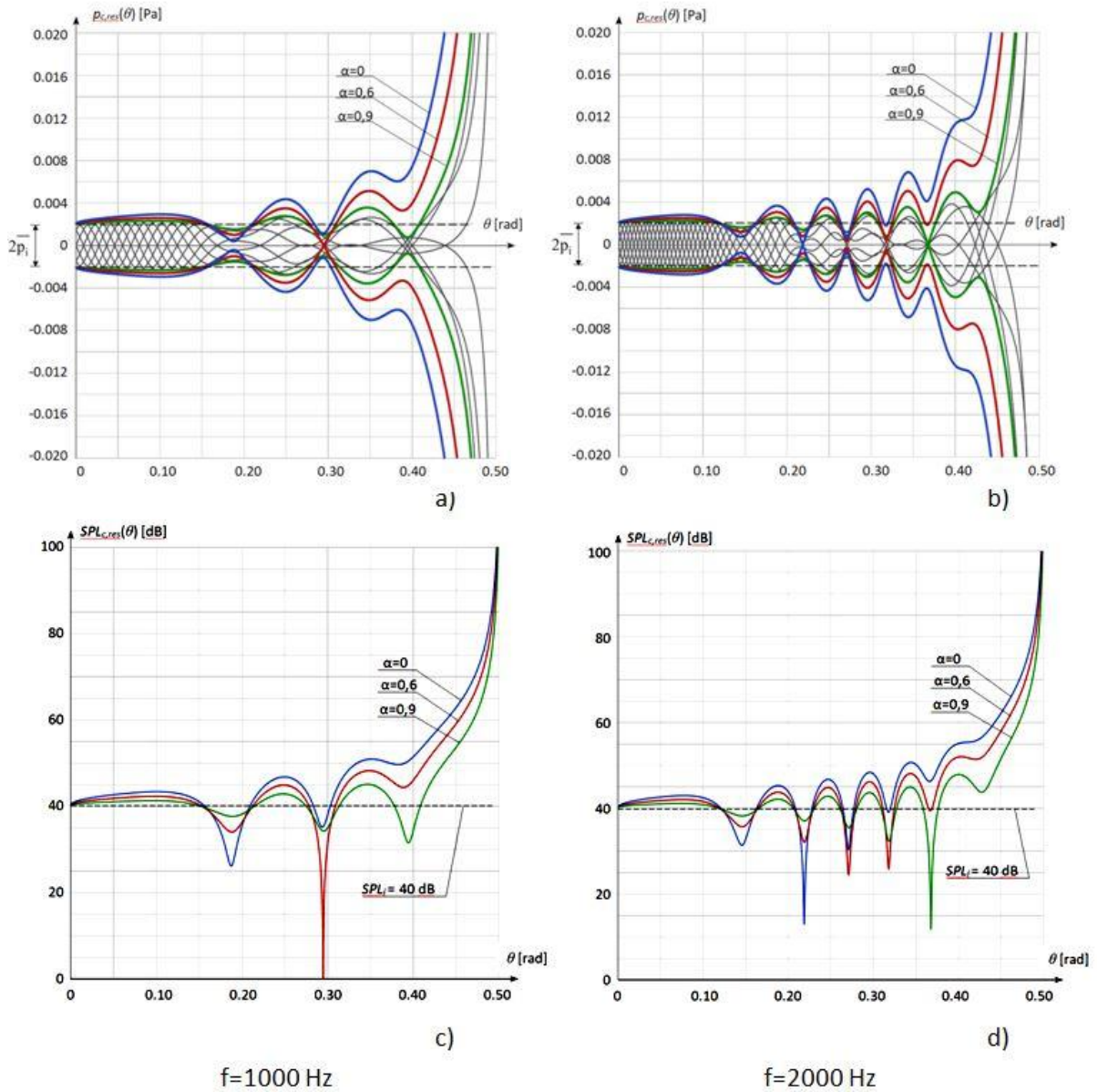
311 
$$SPL_i = 20 \log(0.002 / (2 * 10^{-5})) = 40 \text{ [dB]} \quad (46)$$

312 The sound pressure  $p_{c,res}$  (Eq. (26)) and the corresponding pressure level  $SPL_{c,res}$  on the caus-  
 313 tic (Eq. (47)) fluctuate around these values. The amplitude of the fluctuations increases with  
 314 the increasing effect of wave condensation on the caustic (Fig. 7 a, b).

315 
$$SPL_{c,res}(\theta) = 20 \log(p_{c,res,max}(\theta) / (2 * 10^{-5})) \quad (47)$$

316 At the cusp of the caustic, the concentrated energy of the reflected waves significantly ex-  
 317 ceeds the energy of the incident wave, which reduces the fluctuation effect (Fig. 7 c, d).

318 The result of interference outside the focus is the arrangement of nodes and antinodes  
 319 formed by the superimposition of incident and reflected waves on the caustics. In real condi-  
 320 tions, its regularity shown in Fig. 7 is disturbed by the broadband nature of the sound and by  
 321 the reverberant field of the room. This is combined with the diffraction of the incident low  
 322 frequency wave at the edge of the canopy. As a result, the presence of caustics in the room is  
 323 usually difficult to detect by hearing, and the audible effect of sound focussed by acoustic  
 324 mirrors is reduced to a point focus of sound.



325

326

327

328

329

330

331

332

Fig. 7. a), b) Resultant sound pressure of the plane waves with the frequencies  $f = 1000$  Hz and  $f = 2000$  Hz, respectively, incident on a hemispherical reflector with the diameter  $R = 1$  m and interfering with the wave that forms the caustic.  $\bar{p}_i$ : amplitude of the incident wave,  $\alpha$ : sound absorption coefficient of the reflector. Thin black lines: sound pressure of the resultant wave  $p_{c, res}(t, \theta)$  at the points in time  $t = 0, T/8, \dots, 7T/8$  where  $T = 1/f$ , at  $\alpha = 0.9$ . Green, red and blue lines: amplitude of fluctuations  $p_{c, res, Max}(\theta)$  at  $\alpha = 0.9$ ,  $\alpha = 0.6$  and  $\alpha = 0$ , respectively. Due to symmetry, the range  $0 \leq \theta \leq \pi/2$  is shown. c), d) Resultant sound pressure level  $SPL_{c, res}(\theta)$  of the interfering waves described above.  $SPL_i$ : level of the incident wave.

333 Fig. 7 shows how much sound amplification can be expected at the cusp of the caus-  
334 tics. When the level of incident sound on the mirror is about 40 dB, which corresponds to e.g.  
335 a quiet conversation (Fig. 7 c, d), the sound level felt in the focus is so high that this phenom-  
336 enon can be used for acoustic demonstrations or for eavesdropping of conversations practiced  
337 in historical times. Fig. 7 shows that in the focus, the surface sound power density may in-  
338 crease by approx. 45 dB or more, which is accounted for by a small part of the canopy. It is a  
339 computational illustration of LdV's concept, as shown in Fig. 2. The opening angle of the  
340 canopy in the original LdV drawing, for obvious reasons not supported by calculations, is  
341 approx.  $10^\circ$ .

342 The field installations found in educational parks are a contemporary implementation  
343 of LdV's observation (Fig. 8b). The whisper caves shown in Fig. 8a, apart from demonstrat-  
344 ing the echo effect [10], also serve as an element of historical park architecture and a place of  
345 shelter from rain. Therefore, their shape is wider than required by the demonstrated phenome-  
346 non of reflection.

347

348

349

350

351

352



a)



b)

353 Fig. 8. Outdoor installations erected to demonstrate acoustic curiosities.

354 a) Eighteenth-century Whispering Grottoes in Oliwa Park, Gdańsk, Poland [10], [14],

355 b) Contemporary outdoor installation made by 3D printing [15], [16], [17]

356

357 There are numerous architectural objects in which caustics are formed in the form

358 shown in LdV's drawings. We are talking here primarily about historical interiors with a sa-

359 cred and ceremonial function, containing large areas in the form of a dome (Fig. 9). Caustics

360 in the described form were also created in 19th-century theaters and concert halls with con-

361 cave vaults, which were the then canon of the neo-renaissance style (Fig. 10) [12].

362



363

364

365

366



367

a)

b)

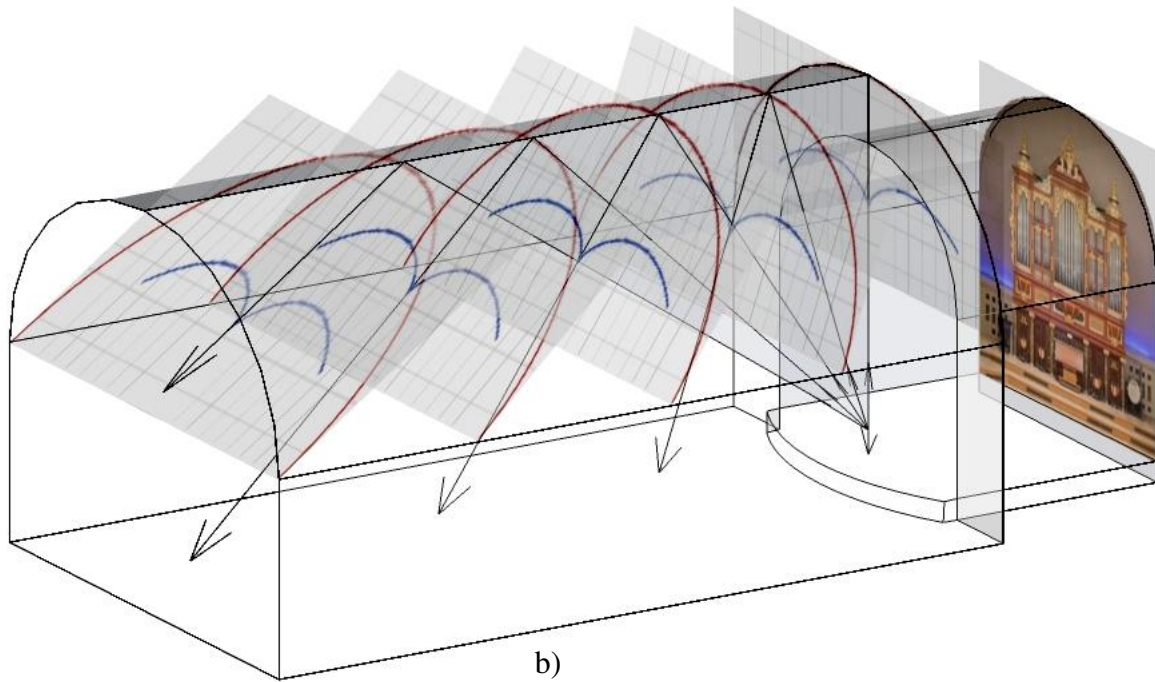
368 Fig. 9. Historical rooms with large dome-shaped areas.

369 a) Hagia Sophia in Istanbul, Turkey, b) Dome of the Rock in Jerusalem, Israel [18]

370



a)



b)

Fig. 10. a) Assembly Hall of Poznań University. This neo-renaissance building was erected according to the design of Edward Fürstenau in 1905-1910, photo courtesy of Poznań Film Commission [19].

b) Cross-sections of a 3D caustic as predicted by LdV [12].

## 372 5.2. Caustics in electromagnetic fields

373 Fig. 11 shows electric field fluctuations on the caustics formed by the reflector of the  
 374 Arecibo radio telescope in Puerto Rico (Fig. 12). The radio telescope was put into operation in  
 375 1963 and initially the reflector aperture was small. It was significantly upgraded in 1997 by  
 376 the use of the Gregorian subreflector system, which concentrates the energy of the caustics  
 377 sections adjacent to the cusp into the single focal point (Fig. 13). The subreflector system con-  
 378 sists of two shaped surfaces called secondary and tertiary reflectors hidden inside on the geo-  
 379 detic dome. The first is the parabolic reflector and the second constitutes the pair of elliptic  
 380 reflectors (Fig. 14) [20].

381 The upgraded aperture of the  $A_{\text{Arecibo}}$  radio telescope is approx.  $30,000 \text{ m}^2$ , which is  
 382 approx. 7% of the hemisphere surface with a radius of  $R_{\text{Arecibo}} = 265 \text{ m}$  (Eq. (48)) [21].

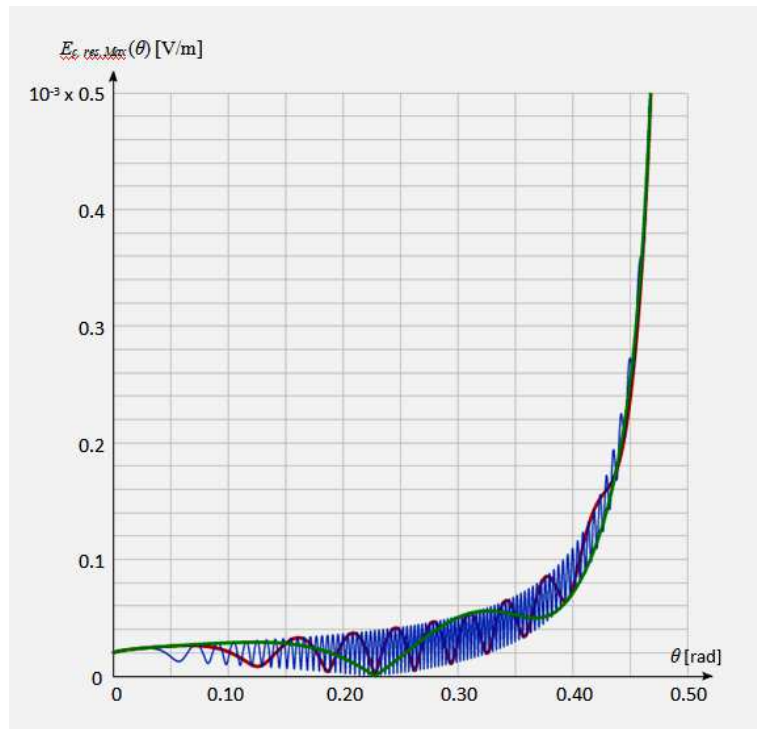
$$383 \quad \frac{A_{\text{Arecibo}}}{2\pi R_{\text{Arecibo}}^2} = \frac{30000}{2\pi 265^2} = 0.068 = 6.8\% \quad (48)$$

384 Compared to the reflector analysed by LdV with an aperture of approx. 0.4% of the hemi-  
 385 sphere area (see Fig. 3, Eqs. (1) and (2)), the relative aperture of the Arecibo radio telescope  
 386 reflector is 17 times greater ( $0.068/0.004 = 17$ ), i.e. by 1 order of magnitude. This is due to the  
 387 fact that, according to LdV, the energy concentrated by the reflector is contained in its focus,  
 388 while the Arecibo radio telescope enlarges it by the energy of a significant part of the caustics.

389 On December 1, 2020 – a tragic day for the scientific community – the Arecibo radio  
 390 telescope was destroyed due to the cables breaking and the 900-ton main platform falling onto  
 391 the radio telescope's canopy.



392  
393  
394  
395  
396  
397  
398  
399



400

401 Fig. 11. Result of the interference of the plane electromagnetic wave incident on a hemispherical re-  
402 flector with the diameter  $R = 265$  m, interfering with the wave reflected from the reflector. Intensity of  
403 the incident wave:  $10^{-12}$  W/m<sup>2</sup>, frequency of the wave: 2 MHz, 10 MHz and 100 MHz (green, red and  
404 blue lines, respectively). Due to symmetry, the range  $0 \leq \theta \leq \pi/2$  is shown.

405

406

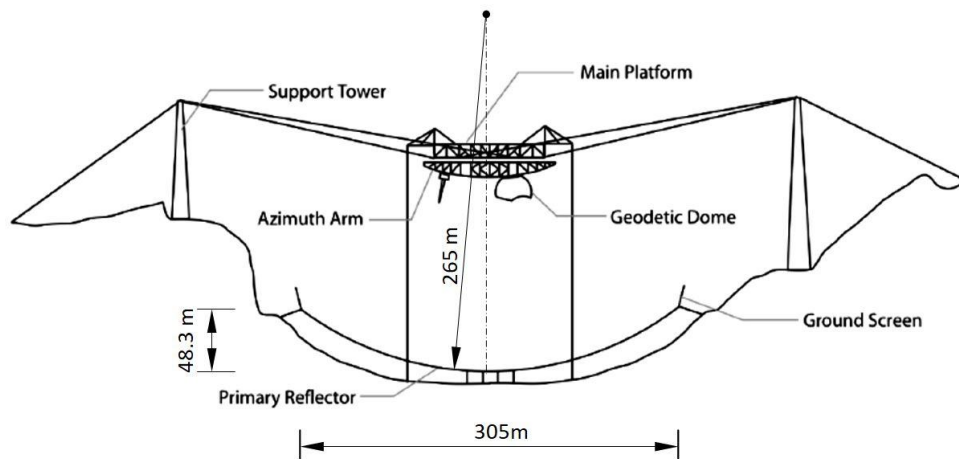
407

408

409

410

411



412

413 Fig. 12. Spherical radio telescope in Arecibo, Puerto Rico, photo taken before 01.12.2020 [22]

414

Below: diagram of the Arecibo telescope [20].

415

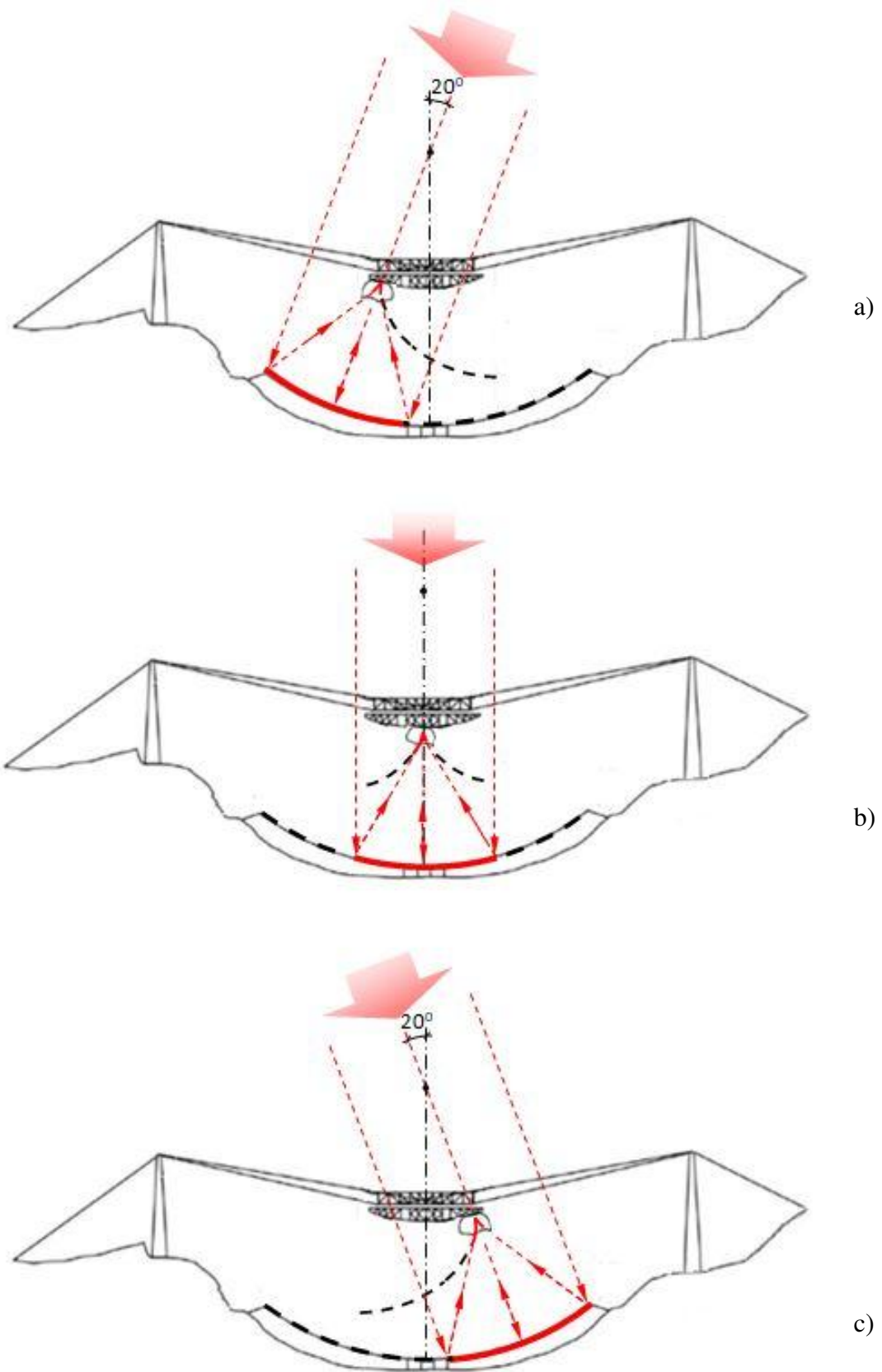
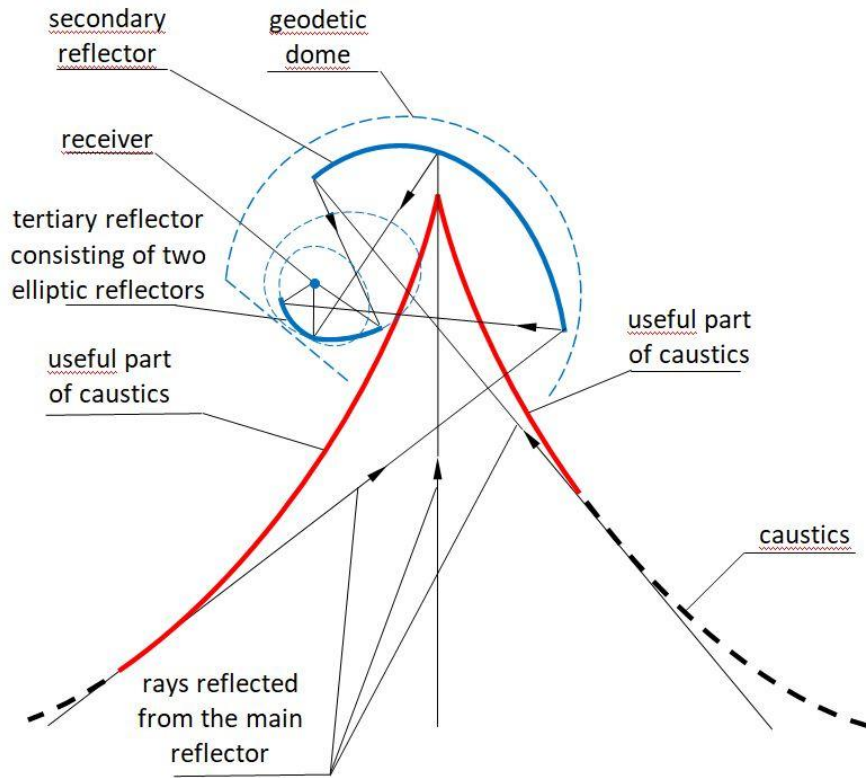


Fig. 13. Bowl of the Arecibo reflector and the caustic it forms. The active part of the reflector and caustics is shown (red). a), b), c): directions of wave arrival  $-20^\circ$ ,  $0^\circ$ ,  $+20^\circ$  relative to the zenith. Illustrative sketch based on [20].

417  
418  
419  
420  
421  
422  
423  
424  
425



426  
427  
428  
429  
430

Fig. 14. Ray tracing of the secondary and tertiary reflectors of the Arecibo

Gregorian Optics [23]. In addition to the energy of the focus, the Gregorian subreflector system also uses the energy concentrated on the part of caustic marked in red. The pair of ellipses defining the shape of the tertiary reflector is shown.

## 431 6. Parabolic reflector

432  
433  
434  
435  
436

In 2016, 53 years after the radio telescope in Arecibo was launched, the FAST radio telescope (Five-hundred-meter Aperture Spherical radio Telescope) was put into operation in Dawodang (China). Its antenna with a diameter of 520 m is a section of a sphere with a radius of  $R_{\text{FAST}} = 300$  m (Fig. 15). A receiver weighing 3 tons, which moves over the dish by a system of cables, enables the observation of radio-sources contained in a cone with an opening

437 angle of aperture of 80 degrees. The FAST radio telescope is a receiving device, while the  
 438 Arecibo radio telescope was a transmitting and receiving device [25].

439 The canopy of the FAST radio telescope consists of 4500 movable elements, the posi-  
 440 tion of which can be corrected in such a way that a selected part of the spherical reflector is  
 441 transformed into a parabolic reflector segment, including a circle with a diameter of 300 m.  
 442 The corrected part of the reflector thus creates an aperture with a diameter of  $A_{\text{FAST}} = 300$  m  
 443 and a depth of  $D_{\text{FAST}} = 40.2$  m [26], which gives an area of approx.  $38,000 \text{ m}^2$ , i.e. approx.  
 444 6.7% of the hemisphere area (Eqs. (49), (50)). This shows a different direction of upgrade of  
 445 LdV's concept over Arecibo. It involves manipulating the curvature of the reflector, while in  
 446 Arecibo, the useful range of the caustics was manipulated.

$$447 \quad 2\Pi \cdot 1 / (2A_{\text{FAST}}) \cdot D_{\text{FAST}} = 2\Pi \cdot 150 \cdot 40.3 \approx 38000 \text{ m}^2 \quad (49)$$

$$448 \quad \frac{38000}{2\Pi R_{\text{FAST}}^2} = \frac{38000}{2\Pi 300^2} = 0.067 = 6.7\% \quad (50)$$

449 The caustics present in the LdV sketches, also known as spherical aberration, are treat-  
 450 ed as a limitation in the use of a spherical mirror. In the case of a parabolic mirror, such a lim-  
 451 itation is a coma aberration. It occurs when the observed object is located off the mirror axis  
 452 and consists in blurring the focus into a loop caustic called a coma (Fig. 17). In a spherical  
 453 mirror, aberration is an irremovable element of its functioning, while in a parabolic mirror, it  
 454 disappears completely with the axial incidence of the rays. In the FAST radio telescope, the  
 455 coma aberration is limited by positioning the receiver with a few-millimetre accuracy, with a  
 456 deviation from the paraboloid axis not exceeding 8 arc seconds [27].

457



458

459

460

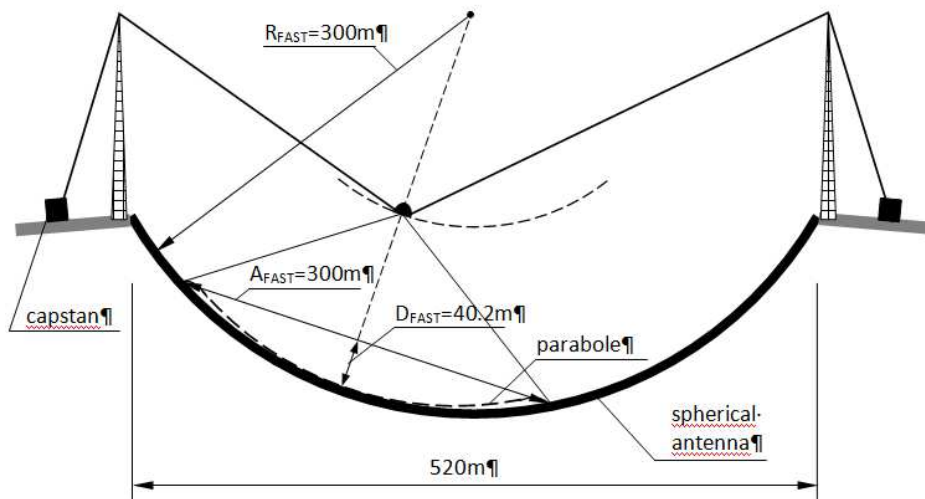
461

462

463

464

465



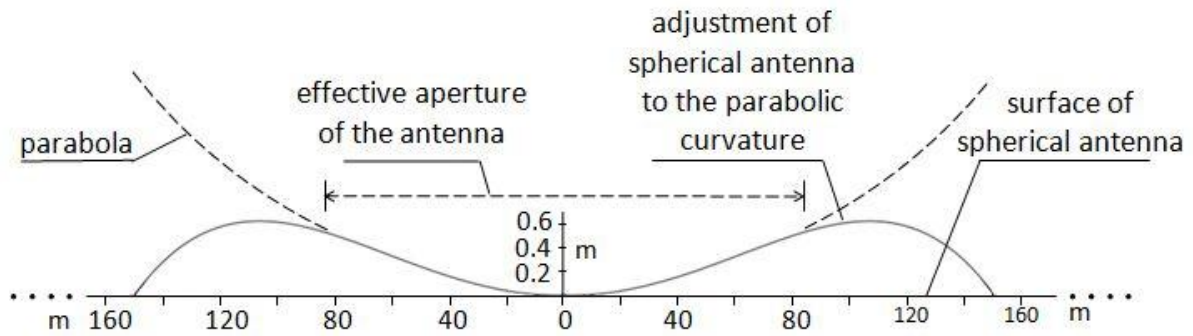
466

Fig. 15. Five-hundred-metre antenna of the FAST radio telescope [24]

467

Below: a diagram of the FAST telescope [27].

468



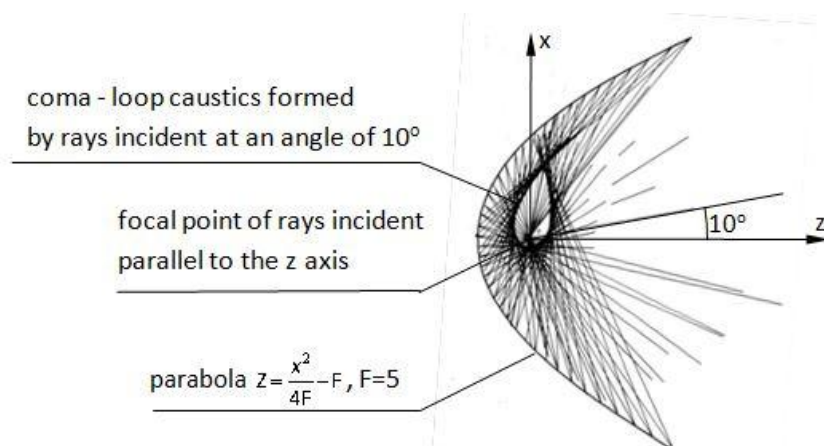
469

470 Fig. 16. One of the tested solutions, showing how to adjust a section of the spherical mirror of the

471

FAST radio telescope to the curvature of the parabola [26].

472



473

474 Fig. 17. Typical distortion of parabolic mirror in the form of comatic aberration. When the source is

475

located off the mirror axis, the focal point takes the form of a loop caustic, known as a coma [28].

476

477 **7. Concluding remarks**

478

In the achievements of many leading fields of science, you can find ideas from hun-

479

dreds of years ago, often coming from areas unrelated to the field. The article shows the pres-

480 ence of the concept of focussing light through a spherical mirror, formulated by Leonardo  
481 daVinci about 500 years ago, in the development of seemingly distant fields of science and  
482 technology, such as acoustics and radio astronomy.

483 Leonardo conducted his theoretical research using a spherical mirror. He showed that  
484 less than 0.5% of the hemisphere area is enough to concentrate energy coming from an infi-  
485 nitely distant source, e.g. from the Sun. With the application of this mirror, the rest of the  
486 canopy is useless. This idea, obvious from the point of view of modern knowledge, but for-  
487 mulated 500 years ago, is present today in many areas of technology and science – the aper-  
488 ture of modern spherical mirrors is only a small part of the hemisphere. Their functioning in  
489 the field of architectural acoustics, in optical instruments, as antennas in radio telescopes, etc.,  
490 is fully in line with the LdV predictions.

491 During the research on the phenomenon of light concentration, LdV showed a method  
492 of graphically determining the surface accompanying the focus, on which the reflected rays  
493 are concentrated. This surface is known today as caustics and is present in many fields of  
494 technology and science. LdV, however, did not develop the idea of caustics, being apparently  
495 unaware of the importance of his discovery. In modern technical knowledge, you can encoun-  
496 ter both of the above-mentioned elements of the functioning of mirrors discovered by LdV,  
497 i.e. foci and caustics. In the example shown in the article, when the caustic energy is added to  
498 the focal energy, the aperture increases from the approx. 0.5% predicted by LdV to approx. 5–  
499 7%. After local adjustment of the spherical mirror surface to the curvature of the parabola, the



500 aperture increases to a similar extent. The aperture of the mirror determined by LdV has  
501 therefore undergone a significant upgrade as a result of the development of receiving tech-  
502 niques. The technical implementation of the described improvements are the 300-metre radio  
503 telescope in Arecibo (Puerto Rico) and the 500-metre FAST radio telescope in Dawodang  
504 (China). Internet reports inform about the concept of building a 1000-metre radio telescope,  
505 located on the dark side of the Moon away from the Earth's electromagnetic smog, but due to  
506 the early stage of this idea, it is not discussed in the article [29].

507         The caustics found in LdV's drawings are also formed in acoustic field indoors. How-  
508 ever, wave phenomena occurring in a room, reverberation and noise floor make it difficult to  
509 audibly identify the caustics. As a result, the effect of sound focussing by large curved surfac-  
510 es in rooms, e.g. arched vaults and concave walls, is reduced to a point focus at the caustic  
511 cusp, and the rest of the caustic becomes invisible. For this reason, the concept of caustics is  
512 almost unknown in the field of architectural acoustics.

513

514

#### 515 **Declaration of competing interest**

516 This research did not receive any specific grant from funding agencies in the public, commer-  
517 cial, or not-for-profit sectors. The author declares that he has no known competing financial  
518 interests or personal relationships that could have appeared to influence the work reported in  
519 this paper.

520

521 **Availability of data and materials**

522 Not applicable

523 **Ethics declarations**

524 **Ethics approval and consent to participate**

525 Not applicable.

526 **Consent for publication**

527 Not applicable.

528

529

## APPENDIX

530

$$\frac{d}{dt} p_{c,res}(t, \theta) = \frac{d}{dt} \left[ \sqrt{I_0 \rho c_s} \left( \sin(\varpi(t + \Delta t_1)) + \sqrt{\frac{2(1-\alpha)\sin(\theta)}{3|\cos^3(\theta)|}} \sin(\varpi(t + \Delta t_2)) \right) \right] = \quad (A.1)$$

$$\sqrt{I_0 \rho c_s} \varpi \left( \cos(\varpi(t + \Delta t_1)) + \sqrt{\frac{2(1-\alpha)\sin(\theta)}{3|\cos^3(\theta)|}} \cos(\varpi(t + \Delta t_2)) \right) = 0$$

531

Substituting

$$\tau = t + \Delta t_1$$

and

$$b = \sqrt{\frac{2(1-\alpha)\sin(\theta)}{3|\cos^3(\theta)|}}$$

(A.2, A.3)

532

yields

$$\cos \varpi(\tau) = -b \cos \varpi(\tau - (\Delta t_1 - \Delta t_2)) \quad (A.4)$$

533

and after expansion

$$\cos \varpi(\tau) = -b [\cos(\varpi\tau) \cos(\varpi(\Delta t_1 - \Delta t_2)) + \sin(\varpi\tau) \sin(\varpi(\Delta t_1 - \Delta t_2))] \quad (A.5)$$

534

regrouping yields

$$\frac{\sin(\varpi\tau)}{\cos(\varpi\tau)} = \frac{\frac{1}{b} + \cos(\varpi(\Delta t_1 - \Delta t_2))}{-\sin(\varpi(\Delta t_1 - \Delta t_2))} \quad (A.6)$$

535

and then

$$\varpi(t + \Delta t_1) = \operatorname{arctg} \left( \frac{\frac{1}{b} + \cos(\varpi(\Delta t_1 - \Delta t_2))}{-\sin(\varpi(\Delta t_1 - \Delta t_2))} \right) \quad (A.7)$$

536

since

$$\Delta t_1 - \Delta t_2 = \frac{\frac{R}{2}(3\sin\theta - 2\sin^3\theta)}{c_s} - \frac{\frac{R}{2}3\sin\theta}{c_s} = -\frac{R\sin^3\theta}{c_s}, \quad (A.8)$$

537

$$t = \frac{1}{\varpi} \operatorname{arctg} \left( \frac{\sqrt{\frac{3|\cos^3\theta|}{2(1-\alpha)\sin\theta}} + \cos\left(\varpi \frac{R\sin^3\theta}{c_s}\right)}{\sin\left(\varpi \frac{R\sin^3\theta}{c_s}\right)} \right) - \Delta t_1 \quad (A.9)$$

538

539 **References**

- 540 [1] [http://www.unmuseum.org/burning\\_mirror.htm](http://www.unmuseum.org/burning_mirror.htm) [29.09.2021].
- 541 [2] <https://en.wikipedia.org/wiki/Ptolemy> [29.09.2021].
- 542 [3] Dominique Raynaud, The aerial perspective of Leonardo da Vinci and his origins in the optics of  
543 Ibn al-haytham (de aspectibus, III, 7) *Arabic Sciences and Philosophy* 19 (2):225-246 (2009).
- 544 [4] Ivanov V.P., Ivanova G.K., Caustic structure of the underwater sound channel. *Open Journal of*  
545 *Acoustics*, **4**, 26-37 (2014) [http://file.scirp.org/pdf/OJA\\_2014032115460011.pdf](http://file.scirp.org/pdf/OJA_2014032115460011.pdf) [29.09.2021].
- 546 [5] Khatkevich A.G., Khatkevich L.A., Propagation of laser beams and caustics in crystals. *Journal of*  
547 *Applied Spectroscopy*, **74**, No. 4 (2007)  
548 <https://link.springer.com/article/10.1007/s10812-007-0086-8> [29.09.2021].
- 549 [6] Skowron J., Analiza niestandardowych zjawisk mikrosoczewkowania grawitacyjnego gwiazd Ga-  
550 laktyki. Rozprawa doktorska (Analysis of non-standard phenomena of gravitational microlensing  
551 of Galactic stars. PhD dissertation, in Polish). Uniwersytet Warszawski (2009)  
552 <http://www.astro.uw.edu.pl/~jskowron/PhD/thesis/phd.pdf> [13.11.2021].
- 553 [7] <http://www.bl.uk/turning-the-pages/?id=cb4c06b9-02f4-49af-80ce540836464a46&type=book>, p.  
554 8–15 The Leonardo notebook, pp. 8–15 [29.09.2021].
- 555 [8] [http://www.bl.uk/turning-the-pages/?id=cb4c06b9-02f4-49af-  
556 80ce540836464a46&type=book,%20p.%208%E2%80%9314](http://www.bl.uk/turning-the-pages/?id=cb4c06b9-02f4-49af-80ce540836464a46&type=book,%20p.%208%E2%80%9314), Leonardo da Vinci's Codex Arun-  
557 del, pp. 224–226, 414 [29.09.2021].
- 558 [9] <http://www.bl.uk/onlinegallery/ttp/leonardo/accessible/pages11and12.html>
- 559 [10] Kulowski A., The caustic in the acoustics of historic interiors. *Applied Acoustics* 133, 82–90  
560 (2018) <https://doi.org/10.1016/j.apacoust.2017.12.008> [29.09.2021].

- 561 [11] <https://www.bl.uk/onlinegallery/ttp/leonardo/accessible/pages13and14.html>
- 562 [12] Kulowski A., Analysis of a caustic formed by a spherical reflector: Impact of a caustic on archi-  
563 tectural acoustics, *Applied Acoustics* 165 (2020),  
564 <https://doi.org/10.1016/j.apacoust.2020.107333> [29.09.2021].
- 565 [13] Burkhard D.G., Shealy D.L., Formula for the density of tangent rays over a caustic surface.  
566 *Applied Optics* vol. 21, No. 18, 3299–06 (1982).
- 567 [14] [https://www.gedanopedia.pl/gdansk/?title=Plik:Park\\_Oliwski\\_Groty.jpg](https://www.gedanopedia.pl/gdansk/?title=Plik:Park_Oliwski_Groty.jpg) [16.08.2020].
- 568 [15] <https://dbt.arch.ethz.ch/project/acoustic-mirrors/> [16.08.2020].
- 569 [16] Kladefira M. et al., Design Strategies for a 3D Printed Acoustic Mirror. Proc. of the 24th  
570 CAADRIA Conference - Vol. 1, Victoria University of Wellington, Wellington, New Zealand, 15–  
571 18 April 2019, pp. 123–132].
- 572 [17] Kladefira M. et al., Printing whisper dishes. Large-scale binder jetting for outdoor installations.  
573 Proc. of the ACADIA 2018 Recalibration: On Imprecision and Infidelity, Proc. of the 38th Annual  
574 Conference of the Association for Computer Aided Design in Architecture, 328–35. Mexico City,  
575 Mexico, October 18-20, 2018.
- 576 [18] <https://www.thoughtco.com/great-domes-from-around-the-world-177717> [29.09.2021].
- 577 [19] <http://poznanimission.pl/lokacja/aula-uam> [21.09.2019].
- 578 [20] [https://www.researchgate.net/figure/A-diagram-of-the-Arecibo-telescope\\_fig1\\_2209614](https://www.researchgate.net/figure/A-diagram-of-the-Arecibo-telescope_fig1_2209614)  
579 [29.09.2021].
- 580 [21] Magnani L., The Arecibo 5GHz Mini-Gregorian Feed System; Spectral Line Performance. Publi-  
581 cations of the Astronomical Society of the Pacific, Vol. 105, No. 690, pp. 894–901, August 1993.

- 582 [22] <https://www.space.com/38217-arecibo-observatory-puerto-rico-telescope-photos.html>  
583 [29.09.2021].
- 584 [23] Cortés-Medellín G., AOPAF: Arecibo Observatory Phased Array Feed. Internet Publication by  
585 National Astronomy and Ionosphere Center Cornell University, Sep 13, 2010  
586 [https://www.naic.edu/~phil/hardware/byuPhasedAr/logs/Cortes%20AOPAF\\_short%20report%20S  
ept%202010-1.pdf](https://www.naic.edu/~phil/hardware/byuPhasedAr/logs/Cortes%20AOPAF_short%20report%20S<br/>587 ept%202010-1.pdf) [29.09.2021].
- 588 [24] <https://www.nature.com/articles/d41586-019-02790-3> [29.09.2021].
- 589 [25] Mathews J.D., (2013), “A short history of geophysical radar at Arecibo Observatory”, History of  
590 Geo- and Space Sciences. Vol. 4(1), pp. 19–33. doi:10.5194/hgss-4-19-2013.  
591 [www.hist-geo-space-sci.net/4/19/2013/hgss-4-19-2013.pdf](http://www.hist-geo-space-sci.net/4/19/2013/hgss-4-19-2013.pdf), doi:10.5194/hgss-4-19-  
592 2013[29.09.2021].
- 593 [26] Nan R., Li D. et al., The Five-Hundred-Meter Aperture Spherical Radio Telescope  
594 (FAST) Project, International Journal of Modern Physics D, ©World Scientific Publishing Compa-  
595 ny, Accepted for publication, <https://arxiv.org/ftp/arxiv/papers/1105/1105.3794.pdf> [29.09.2021].
- 596 [27] Williams II R.L., “Five-Hundred Meter Aperture Spherical Radio Telescope (FAST) Cable-  
597 Suspended Robot Model and Comparison with the Arecibo Observatory”, Internet Publication,  
598 [www.ohio.edu/people/williar4/html/pdf/FAST.pdf](http://www.ohio.edu/people/williar4/html/pdf/FAST.pdf), July 2015. [29.09.2021].
- 599 [28] Schmidt R.F., Analytical caustic surfaces. NASA Technical Memorandum 87805.  
600 NASA Technical Reports Server; April 1987. [https://ntrs.nasa.gov/archive/nasa/  
601 casi.ntrs.nasa.gov/19880001678.pdf](https://ntrs.nasa.gov/archive/nasa/casi.ntrs.nasa.gov/19880001678.pdf) [29.09.2021].
- 602 [29] [https://www.nasa.gov/directorates/spacetech/niac/2020\\_Phase\\_I\\_Phase\\_II/lunar\\_crater\\_radio\\_telescope/  
603 \[26.10.2021\].](https://www.nasa.gov/directorates/spacetech/niac/2020_Phase_I_Phase_II/lunar_crater_radio_telescope/)